

Technical Note: Corrosion and Cavitation Erosion Behaviors of the Thermo-Mechanically Affected Zone (TMAZ) in a Friction Stir Processed Ni-Al Bronze

Q.N. Song,^{†,*} Y.F. Bao,^{*} Y.F. Jiang,^{*} Y.G. Zheng,^{**} D.R. Ni,^{***} and Z.Y. Ma^{***}

ABSTRACT

The microstructure, corrosion, and cavitation erosion behaviors of the thermo-mechanically affected zone (TMAZ) in a friction stir processed Ni-Al bronze were investigated. The TMAZ mainly contained elongated α , refined κ_{II} , β' , and a small portion of eutectoid microstructure $\alpha + \kappa_{III}$. In 3.5 wt% NaCl solution, both the corrosion and cavitation erosion resistance ranked in the order: the cast substrate < the TMAZ < the stirred zone (SZ). Compared with the cast substrate, the TMAZ suffered less severe corrosion as a result of the reduction of eutectoid microstructure, which was susceptible to corrosion, and it was less severely damaged under cavitation erosion because it possessed higher hardness and exhibited more plastic deformation behavior. The SZ was more corrosion and cavitation erosion resistant than the TMAZ because it had the most homogeneous microstructure.

KEY WORDS: cavitation erosion, corrosion, friction stir processing, microstructure, Ni-Al bronze, thermo-mechanically affected zone

INTRODUCTION

Ni-Al bronze (NAB) is a copper-based alloy with the addition of up to 6 wt% each of iron and nickel, 9 wt% to 12 wt% aluminum, and 1 wt% manganese. It has been extensively used in marine applications, especially for making ship propellers because of its excellent combination of corrosion resistance and mechanical properties. Ship propellers rotate at high speeds in seawater and suffer both corrosion and cavitation erosion damage. Large-sized ship propellers are generally castings which contain coarse and heterogeneous microstructure and inevitable porosities. The cast microstructure and defects are detrimental to the mechanical properties, corrosion, and cavitation erosion resistance, and will consequently shorten the lifetime of propellers.

Friction stir processing (FSP) is a novel solid-state surface working technique originated from friction stir welding (FSW).¹ It was reported that FSP eliminated the porosities, refined the microstructure, and improved both the strength and ductility of the cast NAB.²⁻⁷ Recently, the corrosion,⁸⁻¹⁰ sliding wear,¹¹ and cavitation erosion¹²⁻¹³ behaviors of the FSP NAB have also been studied. However, in these studies, it was the center zone of the FSP NAB, i.e., the stirred zone (SZ) that was mainly investigated.

An entire FSW/FSP region contains an SZ, a thermo-mechanically affected zone (TMAZ), a heat affected zone (HAZ), and the substrate. The most severe plastic deformation and adiabatic heating occur in the SZ. Adjacent regions that undergo less severe plastic deformation and heating comprise the TMAZ.

Submitted for publication: April 28, 2016. Revised and accepted: July 28, 2016. Preprint available online: July 28, 2016. <http://dx.doi.org/10.5006/2126>.

[†] Corresponding author. E-mail: qnsong@hhu.edu.cn.

^{*} College of Mechanical and Electrical Engineering, Hohai University, 200 Jinling North Road, Changzhou 213022, China.

^{**} Key Laboratory of Nuclear Materials and Safety Assessment, Institute of Metal Research, Chinese Academy of Sciences, 62 Wencui Road, Shenyang 110016, China.

^{***} Shenyang National Laboratory for Materials Science, Institute of Metal Research, Chinese Academy of Sciences, 72 Wenhua Road, Shenyang 110016, China.

The HAZ is only heated and no deformation occurs.¹⁴ It was reported that the TMAZ, HAZ, and the interfaces between different zones in a FSW/FSP region possessed lower hardness,¹⁵⁻¹⁶ tensile strength,¹⁶ and corrosion resistance.¹⁷⁻²⁰ Fuller, et al., suggested that ductility was at a minimum in the TMAZ under the tool shoulder or along the TMAZ/SZ interface, and a mixture of microvoid formation and cracking was found at the TMAZ/SZ interface in the FSP NAB.⁶ However, it is not clear whether the TMAZ will be the most susceptible zone to corrosion and cavitation erosion attack. The corrosion and cavitation erosion behaviors of the cast substrate and SZ in the FSP NAB have already been studied in previous studies.^{10,13} Therefore, in the present study, the corrosion and cavitation erosion behaviors of the TMAZ were mainly investigated, and comparisons were made among the TMAZ, SZ, and cast substrate.

EXPERIMENTAL PROCEDURES

An as-cast UNS C95800⁽¹⁾ NAB (chemical composition in wt%: Al 9.18, Ni 4.49, Fe 4.06, Mn 1.03, and Cu balance) with a dimension of 300 mm × 70 mm × 8 mm was subjected to FSP. A stirring tool made of nickel-based alloy was used, with a concave shoulder 24 mm in diameter and a threaded conical pin 8 mm in root diameter and 7 mm in length. The rotating rate, traverse speed, and tilt angle of the tool were 1,500 rpm, 50 mm/min, and 3°, respectively. Blowing air was used to cool the tool and processed plate. The cross section of the FSP NAB was polished, etched with a solution containing 5 g of FeCl₃, 2 mL of HCl, and 95 mL of C₂H₅OH, and then observed using an optical microscope. The hardness values of different zones were measured using a Vickers microhardness tester with a load of 300 g and a dwell time of 15 s. A minimum of 15 points were randomly selected for each zone to ensure reproducibility.

Electrochemical measurements were conducted at room temperature (i.e., about 25°C) in a typical three-electrode system using Gamry Interface 1000[†]. A platinum plate and a saturated calomel electrode (SCE) served as the counter and reference electrode, respectively. The test medium was aerated 3.5 wt% NaCl solution prepared from analytical-grade reagent and distilled water. Polarization curves were recorded at a sweep rate of 0.5 mV/s from -0.3 V to 1.2 V versus the open-circuit potential.

The cross section of the FSP NAB was immersed in aerated 3.5 wt% NaCl solution at room temperature for 2 months. It was then transferred to a solution containing 500 mL of distilled water and 500 mL of hydrochloric acid for 2 min to remove the corrosion

products. A scanning electron microscope (SEM, FEI-Inspect F[†], acceleration voltage 25 kV) was used to observe the morphologies.

Cavitation erosion tests were performed in aerated 3.5 wt% NaCl solution using an ultrasonically vibratory apparatus according to ASTM Standard G32.²¹ The frequency and amplitude of the vibrating horn were 20 kHz and 60 μm, respectively. The tested sample was held 0.5 mm below the horn and immersed 15 mm below the surface of the medium. The medium was kept at about 20°C by cycling cooling water. The damaged sample surface after cavitation erosion for different periods was observed by SEM. For both the long-term immersion and cavitation erosion tests, two parallel samples were investigated in order to ensure reproducibility.

RESULTS AND DISCUSSION

Microstructure Evolution

Figure 1 shows the optical cross-sectional macrograph of the FSP NAB and the microstructures of the as-cast substrate, SZ, and TMAZ. No obvious HAZ is found. The cast substrate is composed of lightly etched coarse Widmanstätten α phase and darkly etched β' and κ phases. The longitudinal length of the α phases reaches 100 μm (Figure 1[c]). In the SZ, fine and equiaxed α and β' phases are evenly distributed and the α phase is 5 μm to 10 μm in size, as shown in Figure 1(e). Elongated α grains which are lightly etched are found in the TMAZ, as presented in Figure 1(d); most of the α phases are less than 50 μm in longitudinal length. This finding indicated that the grain size of the α phases ranked in the order: the cast substrate > TMAZ > SZ. During FSP, the primary cast microstructure was elongated along the direction of plastic flow, which was caused by the tool stirring. In the SZ, the elongated grains underwent complete recrystallization and transformed to equiaxed grains. However, in the TMAZ, the deformed grains underwent incomplete recrystallization because of the relatively lower temperature. Therefore, elongated microstructure was mainly found in the TMAZ, and some equiaxed α grains about 10 μm in size were also found, as seen in Figure 1(d).

Figure 2 presents the back scattered electron (BSE) images of the TMAZ microstructure. It can be seen that some κ_{II} phases are only about 1 μm in size, but some are in comparable size with those in the cast substrate. Fine κ_{IV} phases much less than 1 μm are dispersed inside the elongated α phases (Figure 2[a]). As seen in Figure 2(b), refined lamellar eutectoid microstructure α + κ_{III} are mainly distributed at the α/β boundaries, and the lamella length is less than 2 μm. The existence of the κ_{II} phases indicated that the peak temperature in the TMAZ during FSP was lower than 930°C.²² Some of the κ_{II} phases were broken because of the stirring of the tool. Moreover, the

⁽¹⁾ UNS numbers are listed in *Metals and Alloys in the Unified Numbering System*, published by the Society of Automotive Engineers (SAE International) and cosponsored by ASTM International.

[†] Trade name.

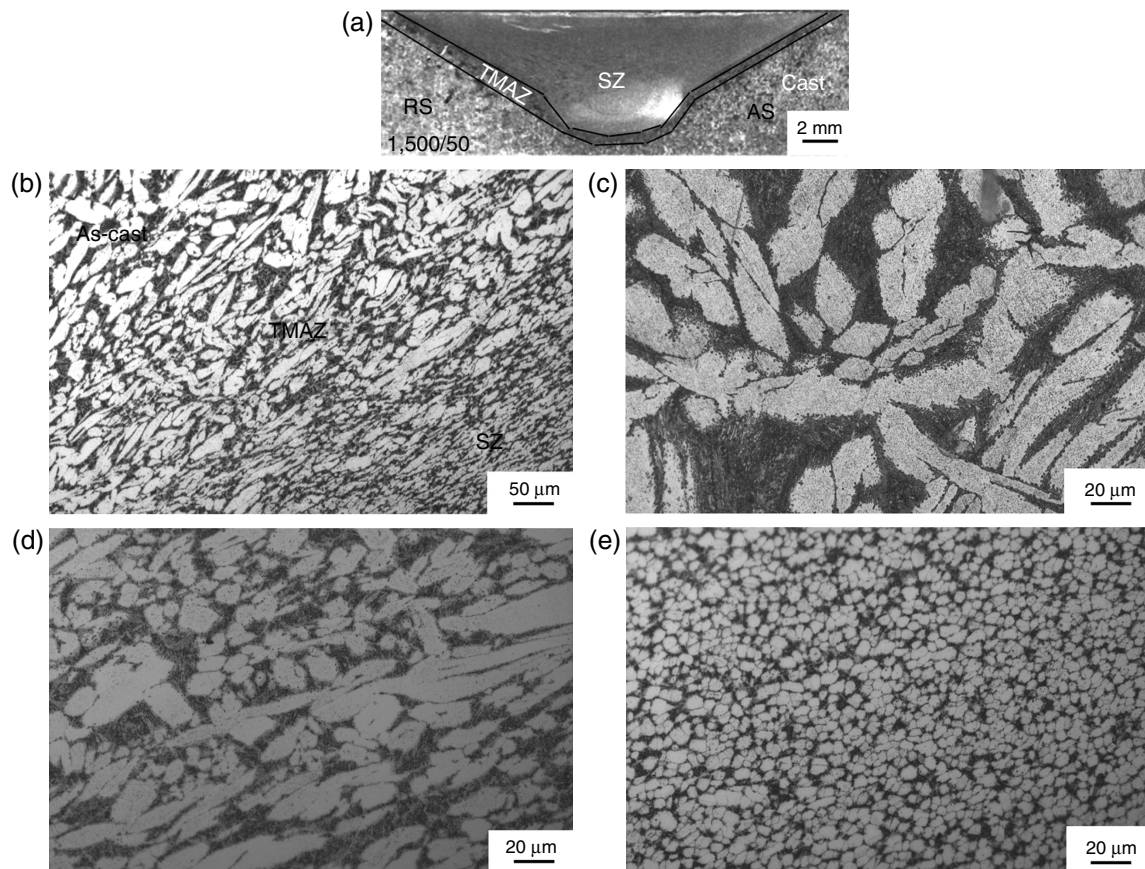


FIGURE 1. (a) Optical macrograph of the FSP NAB 1,500/50 and microstructures of different positions: (b) transitional interface, (c) cast substrate, (d) TMAZ, and (e) SZ.

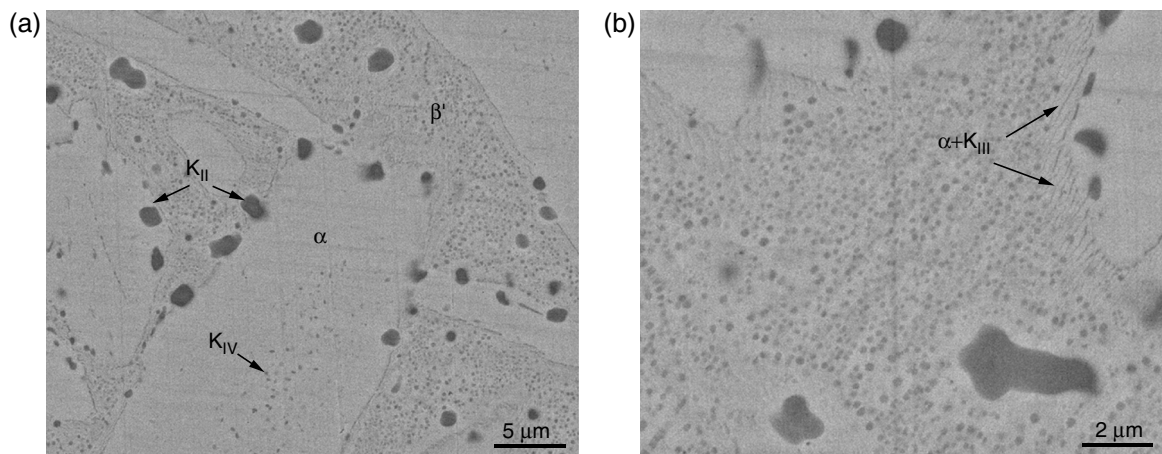


FIGURE 2. BSE images of the TMAZ in the FSP NAB 1,500/50 in (a) smaller and (b) larger magnifications.

existence of the eutectoid microstructure $\alpha + \kappa_{III}$ further demonstrated that the peak temperature in the TMAZ was slightly higher than 800°C .²² Similar findings can be seen in the studies of Oh-Ishi and McNelley.³⁻⁴ In the TMAZ, the eutectoid microstructure $\alpha + \kappa_{III}$ were partially dissolved in the heating

process and subsequently transformed to β' phases, and the remaining eutectoid microstructure was broken because of the stirring of the tool.

The cast microstructure was heterogeneous and the hardness value was about 173 HV for the coarse Widmanstätten α phases, but about 185 HV for

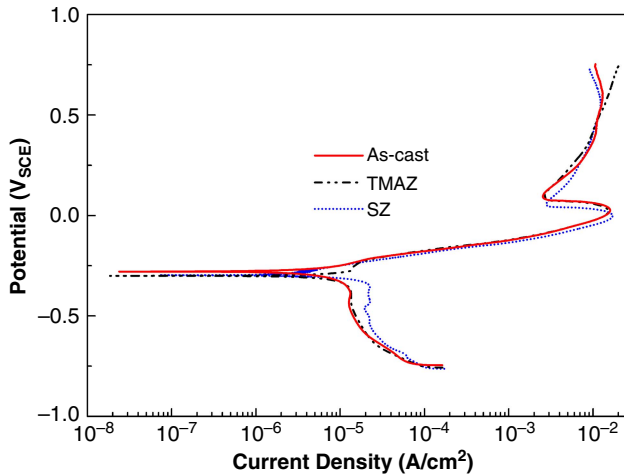


FIGURE 3. Polarization curves of the cast substrate, TMAZ, and SZ in the FSP NAB in 3.5 wt% NaCl solution.

microstructures containing the eutectoid microstructure and κ_{II} phases. The hardness values of the equiaxed microstructure in the SZ and the elongated microstructure in the TMAZ were about 210 HV and 195 HV, respectively. The refined microstructures contributed to higher hardness for the SZ and TMAZ.

Corrosion Behavior in 3.5 wt% NaCl Solution

Figure 3 illustrates the polarization curves of the cast substrate, SZ, and TMAZ in 3.5 wt% NaCl solution. The anodic branches of the three zones are nearly overlapped, demonstrating that the three zones underwent similar anodic dissolution process and exhibited similar initial corrosion behavior. In order to investigate the long-period corrosion behavior, the immersion test was conducted. Figures 4 and 5 present the surface and cross-section morphologies of the three zones with the corrosion products removed after immersion in 3.5 wt% NaCl solution for 2 months. For the cast substrate and TMAZ, the eutectoid

microstructure $\alpha + \kappa_{III}$ and β' phases are preferentially corroded, and pits are mainly found at these phases. The eutectoid microstructure was susceptible to corrosion as the anode (i.e., the lamellar α) and the cathode (i.e., κ_{III}) were alternately distributed.²³ Pits with sizes of 10 μm and 5 μm are found on the surface (Figures 4[a] and [b]), and the pit depth reaches 3.6 μm and 3 μm (Figures 5[a] and [b]) for the cast substrate and TMAZ, respectively. In the TMAZ, the eutectoid microstructures that were susceptible to corrosion were partly dissolved and the remaining parts were refined because of the deformation during FSP; therefore, the TMAZ suffered less severe

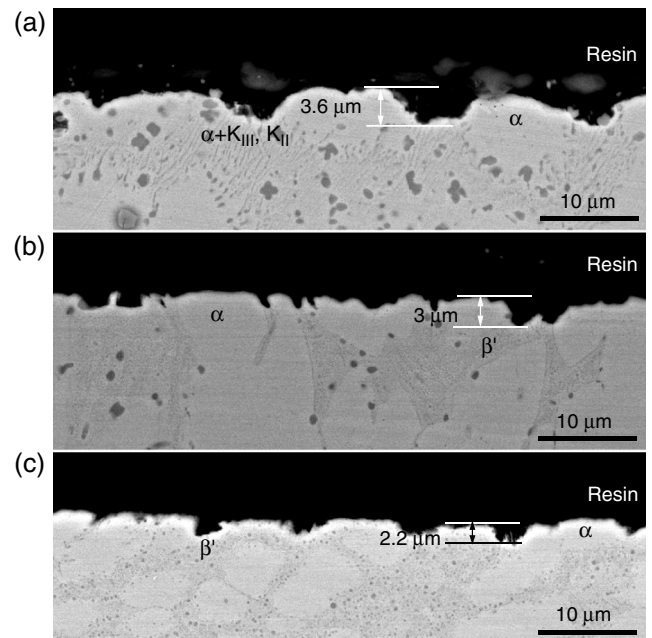


FIGURE 5. Cross-section morphologies of the (a) cast substrate, (b) TMAZ, and (c) SZ in the FSP NAB after immersion in 3.5 wt% NaCl solution for 2 months.

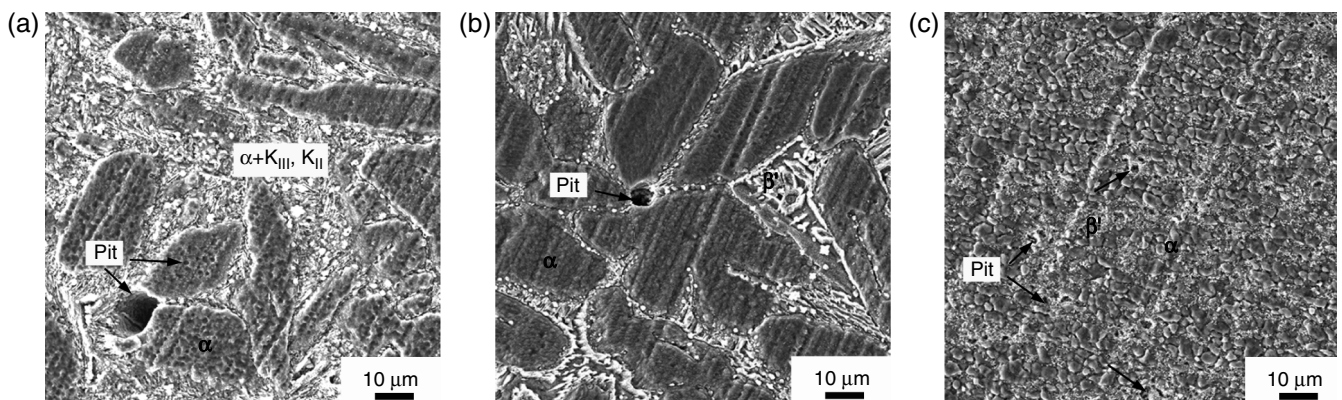


FIGURE 4. Surface morphologies of the (a) cast substrate, (b) TMAZ, and (c) SZ in the FSP NAB after immersion in 3.5 wt% NaCl solution for 2 months with the corrosion products removed.

corrosion than the cast substrate. Considering that SZ possessed the most homogeneous and refined microstructure, general corrosion occurred on the surface. The pit depth only reached 2.2 μm , as presented in Figure 5(c). The above findings indicated that the corrosion resistance of the TMAZ was higher than that of the cast substrate, but lower than that of the SZ.

Cavitation Erosion Behavior in 3.5 wt% NaCl Solution

Figures 6 through 8 show the surface morphologies of the three zones after cavitation erosion in 3.5 wt% NaCl solution for different periods. After cavitation erosion for 30 min, cracks appeared at the α/κ boundaries and shallow cavities exist for the cast substrate, as presented in Figure 6(a). Similar findings can also be found in the study of Al-Hashem, et al.²⁴ However, for the TMAZ and SZ, as seen in Figures 6(b) and (c), extrusions are found at the α phases, indicating that plastic deformation occurred on the surface under the cavitation stress. During FSP, the α phases were elongated and twins formed inside because of the deformation in the TMAZ. Under the cavitation

stress, extrusions formed along these twins' boundaries. After cavitation erosion for 3 h, as shown in Figure 7, severe damage occurs and cavities form at the soft α phases for all three of the zones, whereas the κ phases in the cast substrate and the β' phases in the TMAZ and SZ suffer less severe damage because of their higher hardness. Ten- μm -wide cavities in large depth already appear on the cast substrate, as indicated by black arrows in Figure 7(a). Wide but shallow cavities are found on the TMAZ (Figure 7(b)), and small-sized cavities are dispersed on the SZ (Figure 7(c)). With the cavitation erosion time increasing, the cavities extended and large grooves formed with cavities joining together. As seen in Figure 8(a), deep cavities are found at the bottom of large grooves for the cast substrate, indicating that damage extended deeply into the matrix. Grooves on the TMAZ and SZ are much smaller in depth, as seen in Figures 8(b) and (c), and the SZ is more uniformly damaged than the TMAZ because it had the most homogeneous microstructure. This finding indicated that the cavitation erosion resistance ranked in the order: SZ > TMAZ > the cast substrate, which was consistent with the hardness result. Moreover, it was

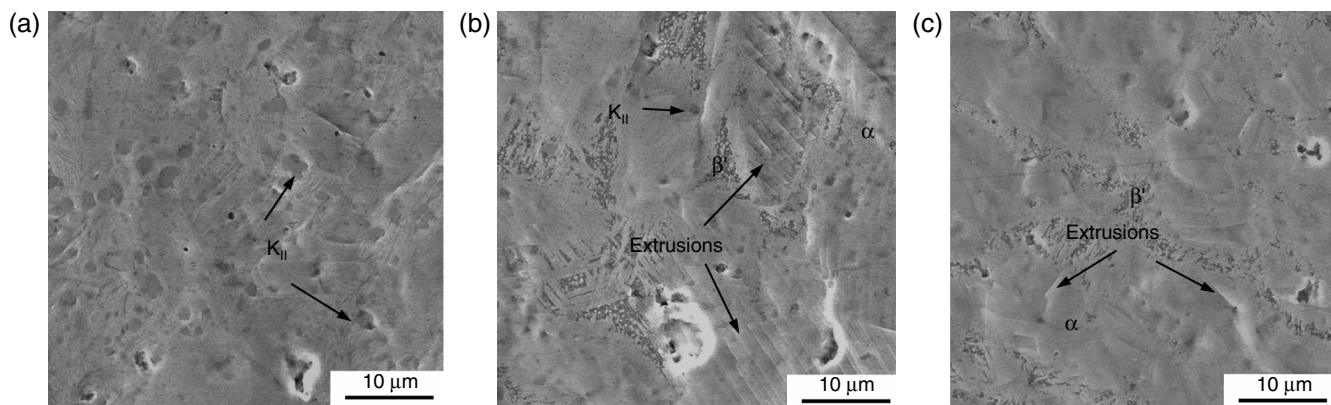


FIGURE 6. Surface morphologies of the (a) cast substrate, (b) TMAZ, and (c) SZ in the FSP NAB after cavitation erosion in 3.5 wt% NaCl solution for 30 min.

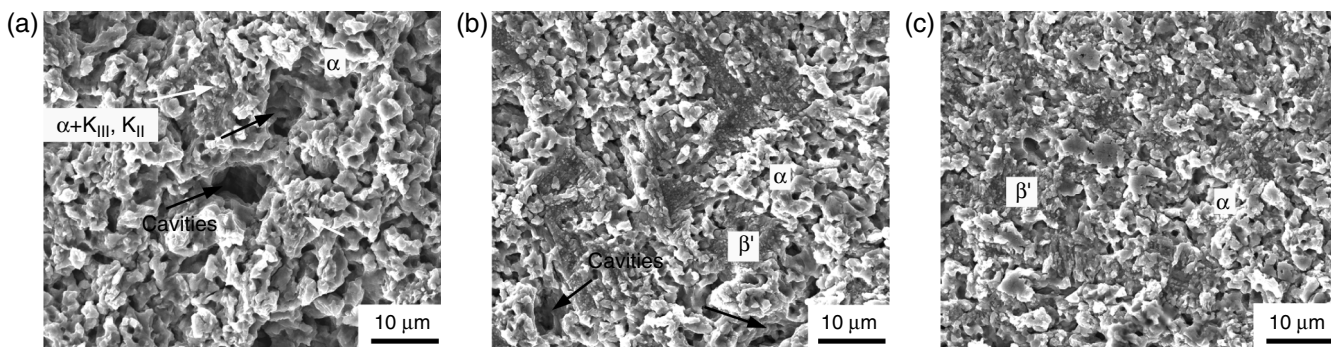


FIGURE 7. Surface morphologies of the (a) cast substrate, (b) TMAZ, and (c) SZ in the FSP NAB after cavitation erosion in 3.5 wt% NaCl solution for 3 h.

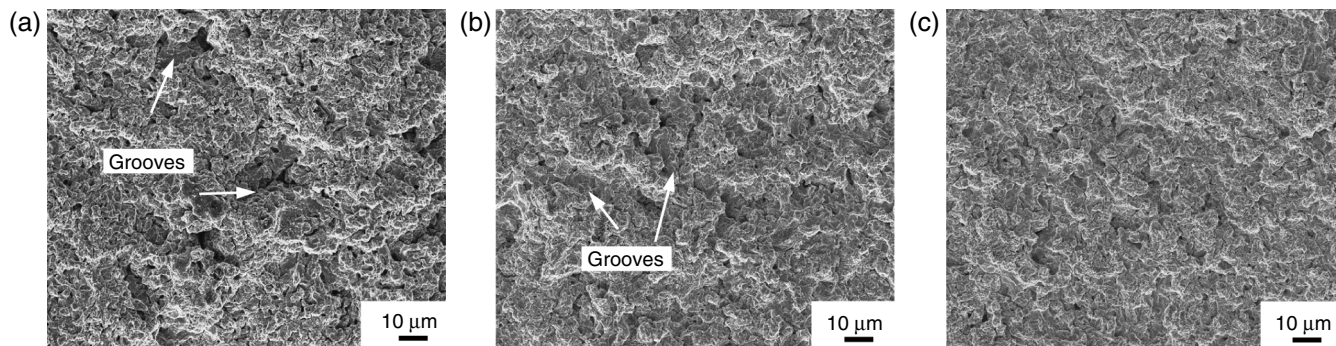


FIGURE 8. Surface morphologies of the (a) cast substrate, (b) TMAZ, and (c) SZ in the FSP NAB after cavitation erosion in 3.5 wt% NaCl solution for 10 h.

reported that the fatigue crack initiated at the cast substrate and then extended to the TMAZ and FSP zone (akin to the SZ here), and the tensile samples failed in the cast microstructure away from the SZ and TMAZ, indicating that the cast substrate possessed inferior fatigue and tensile strength compared with the TMAZ and SZ.²⁵ Higher fatigue and tensile strength generally contributed to higher cavitation erosion resistance.²⁶⁻²⁷ Therefore, it was the cast substrate rather than the TMAZ that suffered the most severe cavitation erosion damage in the entire FSP NAB region.

From the above, both the corrosion and cavitation erosion resistance in 3.5 wt% NaCl solution ranked in the order: SZ > TMAZ > the cast substrate. This indicated that the transitional zone, i.e., the TMAZ, was not the most susceptible zone to corrosion and cavitation erosion damage in the FSP NAB.

CONCLUSIONS

- ❖ The TMAZ in the FSP NAB located between the cast substrate and SZ. It mainly contained elongated α , β' , refined κ_{II} phases, and a small portion of eutectoid microstructure $\alpha + \kappa_{III}$.
- ❖ Polarization curves indicated that the TMAZ exhibited similar initial corrosion behavior with the cast substrate and SZ. Long-period immersion test results demonstrated that the TMAZ suffered less severe corrosion than the cast substrate as a result of the reduction of eutectoid microstructure $\alpha + \kappa_{III}$, which were susceptible to corrosion. The SZ was more corrosion resistant than the TMAZ because it had the most homogeneous microstructure.
- ❖ The SZ possessed the highest cavitation erosion resistance, followed by the TMAZ and cast substrate. This result was consistent with the rank order of hardness. More plastic deformation behavior under cavitation stress also contributed to the superior cavitation erosion resistance of the TMAZ, compared with the cast substrate.

In conclusion, the TMAZ was not the most susceptible zone in the entire FSP NAB region to corrosion

and cavitation erosion damage in 3.5 wt% NaCl solution.

ACKNOWLEDGMENTS

This research was financially supported by Fundamental Research Funds for the Central Universities of P.R. China (No. 2014B11614 and No. 2015B10126).

REFERENCES

1. W.M. Thomas, E.D. Nicholas, J.C. Needham, M.G. Murch, P. Temple-Smith, C.J. Dawes, "Friction-Stir Butt Welding," G.B. Patent 9125978.8, 1991.
2. W.A. Palko, R.S. Fielder, P.F. Young, *Mater. Sci. Forum* 426-432 (2003): p. 2909.
3. K. Oh-Ishi, T.R. McNelley, *Metall. Mater. Trans. A* 35 (2004): p. 2951.
4. K. Oh-Ishi, T.R. McNelley, *Metall. Mater. Trans. A* 36 (2005): p. 1575.
5. D.R. Ni, P. Xue, D. Wang, B.L. Xiao, Z.Y. Ma, *Mater. Sci. Eng. A* 524 (2009): p. 119.
6. M.D. Fuller, S. Swaminathan, A.P. Zhilyaev, T.R. McNelley, *Mater. Sci. Eng. A* 463 (2007): p. 128.
7. C.B. Fuller, M.W. Mahoney, W.H. Bingel, M. Calabrese, B. London, *Mater. Sci. Forum* 539-543 (2007): p. 3751.
8. D.R. Ni, B.L. Xiao, Z.Y. Ma, Y.X. Qiao, Y.G. Zheng, *Corros. Sci.* 52 (2010): p. 1610.
9. Y.T. Lv, L.Q. Wang, X.Y. Xu, W.J. Lu, *Metals* 5 (2015): p. 1695.
10. Q.N. Song, Y.G. Zheng, D.R. Ni, Z.Y. Ma, *Corrosion* 71 (2015): p. 606.
11. S. Thapliyal, D.K. Dwivedi, *Tribol. Int.* 97 (2016): p. 124.
12. A. Ahmad, H. Li, Z. Pan, D. Cuiuri, S. Van Duin, N. Larkin, J. Polden, N. Lane, *Metall. Mater. Trans. B* 45 (2014): p. 2291.
13. Q.N. Song, Y.G. Zheng, S.L. Jiang, D.R. Ni, Z.Y. Ma, *Corrosion* 69 (2013): p. 1111.
14. R.S. Mishra, Z.Y. Ma, *Mater. Sci. Eng. R* 50 (2005): p. 1.
15. L.H. Wu, D. Wang, B.L. Xiao, Z.Y. Ma, *Scrip. Mater.* 78-79 (2014): p. 17.
16. N. Afrin, D.L. Chen, X. Cao, M. Jahazi, *Mater. Sci. Eng. A* 472 (2008): p. 179.
17. J.B. Lumsden, M.W. Mahoney, C.G. Rhodes, G.A. Pollock, *Corrosion* 59 (2003): p. 212.
18. M. Jariyaboon, A.J. Davenport, R. Ambat, B.J. Connolly, S.W. Williams, D.A. Price, *Corros. Sci.* 49 (2007): p. 877.
19. J. Kang, Z. Feng, G.S. Frankel, J. Li, G. Zou, A. Wu, *Corrosion* 72 (2016): p. 719.
20. Y. Savguira, W.H. Liu, D.J. Miklas, T.H. North, S.J. Thorpe, *Corrosion* 70 (2014): p. 858.

21. ASTM G32-03, "Standard Test for Cavitation Erosion Using Vibratory Apparatus" (West Conshohocken, PA: ASTM International, 2003).
22. E.A. Culpan, G. Rose, *J. Mater. Sci.* 13 (1978): p. 1647.
23. E.A. Culpan, G. Rose, *Br. Corros. J.* 14 (1979): p. 160.
24. A. Al-Hashem, P.G. Caceres, W.T. Riad, H.M. Shalaby, *Corrosion* 51 (1995): p. 331.
25. A. Nolting, L.M. Cheng, J. Huang, *J. ASTM Int.* 5 (2008): p. 1.
26. W. Będkowski, G. Gasiak, C. Lachowicz, A. Lichtarowicz, T. Łagoda, E. Macha, *Wear* 230 (1999): p. 201.
27. R.H. Richman, W.P. McNaughton, *Wear* 140 (1990): p. 63.